Transmembrane protein OSTA-1 shapes sensory cilia morphology via regulation of intracellular membrane trafficking in *C. elegans*

Anique Olivier-Mason[1], Martin Wojtyniak[1], Rachel V. Bowie[2], Inna V. Nechipurenko[1], Oliver E. Blacque[2] and Piali Sengupta[1,*]

SUMMARY

The structure and function of primary cilia are critically dependent on intracellular trafficking pathways that transport ciliary membrane and protein components. The mechanisms by which these trafficking pathways are regulated are not fully characterized. Here we identify the transmembrane protein OSTA-1 as a new regulator of the trafficking pathways that shape the morphology and protein composition of sensory cilia in *C. elegans*. *osta-1* encodes an organic solute transporter alpha-like protein, mammalian homologs of which have been implicated in membrane trafficking and solute transport, although a role in regulating cilia structure has not previously been demonstrated. We show that mutations in *osta-1* result in altered ciliary membrane volume, branch length and complexity, as well as defects in localization of a subset of ciliary transmembrane proteins in different sensory cilia types. OSTA-1 is associated with transport vesicles, localizes to a ciliary compartment shown to house trafficking proteins, and regulates both retrograde and anterograde flux of the endosome-associated RAB-5 small GTPase. Genetic epistasis experiments with sensory signaling, exocytic and endocytic proteins further implicate OSTA-1 as a crucial regulator of ciliary architecture via regulation of cilia-destined trafficking. Our findings suggest that regulation of transport pathways in a cell type-specific manner contributes to diversity in sensory cilia structure and might allow dynamic remodeling of ciliary architecture via multiple inputs.

KEY WORDS: *Caenorhabditis elegans*, Cilia, Organic solute transporter, Trafficking

INTRODUCTION

Primary non-motile cilia are now widely recognized as crucial cellular signaling centers (Bisgrove and Yost, 2006; Singla and Reiter, 2006). Cilia emanate from the cell surface and contain a microtubule-based axoneme surrounded by a specialized membrane. The ciliary membrane concentrates receptors, channels and other membrane-associated proteins required for sensing environmental cues (e.g. Liu et al., 2007; Mayer et al., 2008). Although the majority of primary cilia are simple rod-like structures, cilia morphology can also be developmentally specialized for specific cellular functions such as phototransduction or olfaction (Silverman and Leroux, 2009). In addition, both cilia architecture and protein composition are highly dynamic and can be modulated by external cues and the internal state (Avasthi and Marshall, 2012; Besschetnova et al., 2010; Goetz et al., 2009; Higginbotham et al., 2012; Mesland et al., 1980; Mukhopadhyay et al., 2008; Pan and Snell, 2005), suggesting that active regulation of cilia morphology is crucial for maintaining cellular homeostasis. The mechanisms that underlie dynamic remodeling of cilia structure and function are not well understood.

Cilia are compartmentalized organelles that restrict access of most non-ciliary proteins via a ciliary 'gate' consisting of the transition zone and the immediately proximal transition fibers at the ciliary base (Czarnecki and Shah, 2012; Fisch and Dupuis-Williams,

2011; Reiter et al., 2012; Satir and Christensen, 2007). Although alternate mechanisms of delivery of transmembrane proteins to cilia have been described (Hunnicutt et al., 1990; Milenkovic et al., 2009), ciliary proteins are largely believed to be trafficked via post-Golgi vesicles to the ciliary base region (Nachury et al., 2010; Papermaster et al., 1985; Pazour and Bloodgood, 2008; Sorokin, 1962). Following fusion of the vesicles with the periciliary membrane, trafficking of membrane and transmembrane protein cargoes into cilia may then be facilitated by motor-driven intraflagellar transport (IFT) (Nachury et al., 2010; Orozco et al., 1999; Pazour and Bloodgood, 2008; Pedersen et al., 2008; Rosenbaum and Witman, 2002). A number of proteins involved in the exocytic delivery of cilia membrane and protein components have been described, including the BBSome complex and the Rab8 small GTPase (Deretic et al., 1995; Jin et al., 2010; Moritz et al., 2001; Nachury et al., 2007). Although the BBSome has been implicated in ciliary protein removal (Lechtreck et al., 2009), we and others have shown that active clathrin-mediated endocytosis also plays an important role in the retrieval of ciliary membrane and maintenance of cilia morphology (Hu et al., 2007; Kaplan et al., 2012). Thus, ciliary structural and functional homeostasis is likely to be maintained in part via a balance between exocytosis and endocytosis, suggesting that the precise regulation of these pathways is crucial for ciliary morphogenesis.

The *C. elegans* hermaphrodite contains sixty ciliated sensory neurons, a subset of which exhibits highly specialized morphologies essential for neuronal functions (Perkins et al., 1986; Ward et al., 1975). As in other organisms, *C. elegans* sensory cilia are formed by IFT and contain receptors, channels and other molecules required for sensory signal transduction (Inglis et al., 2007). We previously showed that the specialized ciliary morphology of the AWB olfactory neuron type is dynamic and can be modulated by sensory

[1]Department of Biology and National Center for Behavioral Genomics, Brandeis University, Waltham, MA 02454, USA. [2]School of Biomolecular and Biomedical Science, UCD Conway Institute, University College Dublin, Belfield, Dublin 4, Ireland.

*Author for correspondence (sengupta@brandeis.edu)

signaling (Mukhopadhyay et al., 2008). Genetic epistasis experiments suggest that sensory signaling might modulate AWB cilia morphology via regulation of trafficking pathways (Kaplan et al., 2012; Mukhopadhyay et al., 2008). However, our understanding of the molecular components of these trafficking pathways and their regulation remains incomplete.

Here we identify OSTA-1 as a new component of the protein trafficking pathways that regulate ciliary morphology in *C. elegans*. *osta-1* encodes a *C. elegans* homolog of the conserved transmembrane organic solute transporter alpha proteins, members of which have been shown to be associated with trafficked vesicles and implicated in membrane and organic solute transport in mammalian secretory cells (Best and Adams, 2009; Best et al., 2008; Malinovsky et al., 2010; Svingen et al., 2007). Mutations in *osta-1* result in defects in morphology and transmembrane protein localization in sensory cilia. We show that OSTA-1 regulates trafficking of the endosome-associated RAB-5 small GTPase in ciliated sensory neuron dendrites and interacts genetically with sensory signaling and trafficking genes to shape ciliary architecture and membrane volume. Identification of OSTA-1 as a new component of ciliary trafficking pathways highlights the mechanistic complexity of this process and suggests that the precise regulation of these pathways contributes to the dynamic remodeling of specialized cilia structure and function.

MATERIALS AND METHODS
C. elegans strains
Animals were maintained on *E. coli* OP50 bacteria using standard procedures (Brenner, 1974). Double-mutant strains were constructed by standard genetic methods and the presence of alleles was verified by PCR-based genotyping and sequencing, or phenotypic analyses. Transgenic strains were generated using *unc-122*p::*dsRed*, *unc-122*p::*gfp* or *elt-2*p::*gfp* as the co-injection marker. A complete list of strains is provided in supplementary material Table S1.

Isolation and identification of *osta-1* alleles
The *oy98* allele was isolated in a *mut-7* mutator-mediated (Ketting et al., 1999) screen for suppressors of downregulated *str-1*p::*gfp* expression in *kin-29(oy39)* animals (A. van der Linden and P.S., unpublished) (Lanjuin and Sengupta, 2002; van der Linden et al., 2007). The *oy98* allele was separated from the *mut-7(pk720)* and *kin-29(oy39)* mutations by outcrossing with wild-type animals, and mapped by standard methods (Davis et al., 2005) to a 3 cM interval on the left arm of linkage group II. The dye-filling phenotype of *oy98* was fully rescued by the WRM0618aD03 fosmid and subsequently by C01B12.4 genomic sequences. The *tm5255* allele was isolated by the National BioResource Project (Japan). The *ttTi4182* allele was generated by the NEMAGENETAG Project funded by the European Community. All alleles were outcrossed at least three times prior to analyses. The nature of the molecular lesions in the three *osta-1* alleles was determined by amplification and sequencing of genomic sequences. *osta-1* cDNAs obtained by reverse transcription of RNA isolated from mutant strains were sequenced to determine the effects of the mutations on *osta-1* transcripts.

Molecular biology
Cell-specific expression constructs were generated by cloning relevant sequences downstream of promoter sequences in a modified pPD95.77 expression plasmid (a gift from A. Fire, Stanford University). Transcriptional and translational fusion genes between *osta-1* and *gfp* sequences were generated by PCR fusion (Hobert, 2002). The *osta-1*p::*gfp* fusion gene contained 2.0 kb of *osta-1* upstream regulatory sequences. The *osta-1*p::*osta-1*::*gfp* construct was generated by amplifying *osta-1* genomic sequences including 2.0 kb upstream, the entire coding region and 0.3 kb of downstream sequence. *osta-1*, *nphp-4*, *rab-5* and *rab-8* cDNAs were obtained by reverse transcription from wild-type RNA. The *nphp-4*p::*nphp-4*::*gfp* plasmid was a kind gift of M. Barr (Rutgers University) (Jauregui

and Barr, 2005). Primer sequences are listed in supplementary material Table S2.

Dye-filling and behavioral assays
Animals were dye filled with DiI as described previously (Herman and Hedgecock, 1990; Perkins et al., 1986) and examined under a compound or spinning disk confocal microscope.

The following sensory behaviors were examined in wild type and *osta-1(tm5255)* and *osta-1(ttTi4182)* mutants: avoidance of a point source of 1:10 dilution of the repellent 2-nonanone (mediated by the AWB neurons) (Troemel et al., 1997); avoidance of 60% glycerol (mediated by the ASH neurons) (Bargmann et al., 1990); and entry into the alternative dauer stage mediated by sensation of small molecule ascarosides by the ASK and ASI neurons (Bargmann and Horvitz, 1991; Kim et al., 2009; McGrath et al., 2011).

General microscopy
For ciliary morphology and protein localization analyses, animals grown at the appropriate temperature were mounted on agarose pads set on microscope slides and anesthetized using 10 mM tetramisole hydrochloride (Sigma) or 50 mM sodium azide (Sigma). Cilia were examined on inverted spinning disk confocal microscopes (Zeiss Axio Observer or Zeiss Axiovert 200M with a Yokogawa CSU-22 spinning disk confocal head). Optical sections were collected using SlideBook 5.0 (Intelligent Imaging Innovations; 3i) software and *z*-projected at maximum intensity unless noted otherwise. Cilia length, morphology measurements and analyses of protein localization were performed using ImageJ software (National Institutes of Health). In all cases, measurements of grouped strains were performed together on at least two independent days.

Dendritic trafficking, IFT analyses and fluorescence recovery after photobleaching (FRAP)
Time-lapse images for dendritic trafficking and IFT analyses were acquired and analyzed essentially as previously described (Kaplan et al., 2012). The flux of particles was calculated as the total number of particles (stationary or mobile in either direction) within an in-focus region of the dendrite (normalized to 22 μm) over the course of 1 minute. The location of the middle segment of each cilium was individually estimated by measuring the total length of each cilium and multiplying by either 0.25 or 0.5 if the cilium was AWB or ASH/ASI, respectively (Mukhopadhyay et al., 2007; Snow et al., 2004). The distal segments were defined as regions of the cilium more distal from the cell soma than the middle segments. In the kymograph analyses, the velocity lines were drawn in the middle of each user-defined segment.

FRAP experiments were performed as described (Kaplan et al., 2012). Fluorescence recovery across images was recorded every 5 seconds when photobleaching the entire ASI cilium, and every 1 second when photobleaching a region within an ASI cilium. Fluorescence intensity measurements and data normalization were performed as described (Kaplan et al., 2012). Quantitation of the mobile fraction (Mf) and the half-time of equilibration ($t_{1/2}$) were calculated as described (Bancaud et al., 2010).

RESULTS
osta-1 mutants exhibit progressive cell type-specific dye-filling defects
Six pairs of neurons in the head amphid sensory organs fill with the lipophilic dye DiI in wild-type animals (Fig. 1A) (Herman and Hedgecock, 1990; Perkins et al., 1986). Mutants with defects in cilia or dendrite morphology frequently exhibit dye-filling defects in some or all dye-filling neurons (Hedgecock et al., 1985; Ou et al., 2007; Perkins et al., 1986; Starich et al., 1995; Williams et al., 2008). In a forward genetic screen designed to identify mutants with defects in sensory neuron structure and function (see Materials and methods) we identified the *oy98* mutant, which exhibited a cell type-specific dye-filling defect (Fig. 1B; Table 1). The ASI and ASK sensory neuron pairs in the amphid consistently failed to dye fill, and the AWB neurons exhibited weaker and more variable dye
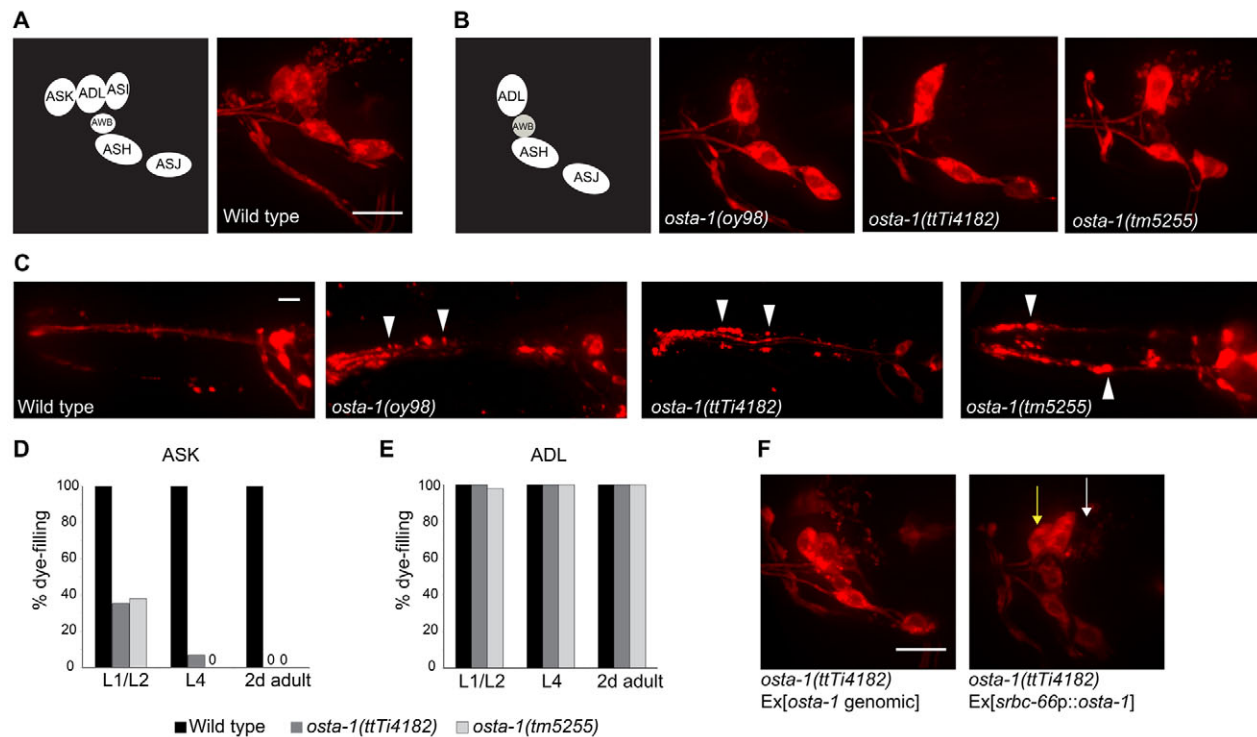
Fig. 1. *C. elegans osta-1* mutants exhibit cell-specific defects in uptake of lipophilic dye. (**A**,**B**) DiI uptake in head amphid organ sensory neurons in wild-type (A) and *osta-1* mutant (B) adults. Schematic interpretations are shown to the left. Side views showing one of each neuron pair; anterior is left. (**C**) *osta-1* but not wild-type adults exhibit punctate dye accumulations (arrowheads) along sensory neuron dendrites. (**D**,**E**) DiI uptake in ASK (D) and ADL (E) in wild type and *osta-1* mutants at the indicated developmental stages. *n*=24-50 animals each. (**F**) The dye-filling defect of *osta-1(ttTi4182)* animals is rescued in all affected neurons (left) or in the ASK (right, yellow arrow) but not ASI neurons (right, white arrow) upon expression of C01B12.4 sequences under its endogenous or the ASK-specific *srbc-66* promoter, respectively. Animals were grown at 20°C. Scale bars: 10 µm.

filling in all *oy98* mutant adults examined (Fig. 1B; Table 1). Although the ASH, ASJ and ADL amphid neurons continued to dye fill (Fig. 1B; Table 1), we observed an accumulation of DiI in a punctate pattern along filled sensory dendrites (Fig. 1C), similar to observations made in animals carrying loss-of-function mutations in a subset of transition zone protein genes (Williams et al., 2008). The *ttTi4182* and *tm5255* mutations were found to be allelic to *oy98*; animals homozygous for these mutations exhibited similar dye-

filling defects and punctate dye accumulation in filled dendrites (Fig. 1B,C; Table 1). We refer to the gene affected by these mutations as *osta-1* (*organic solute transporter alpha homolog 1*; see below).

To determine whether the observed dye-filling phenotypes reflected defects in the generation or maintenance of neuronal morphology, we examined the ability of *osta-1* larvae to dye fill. The ASK neurons exhibited a partially age-dependent dye uptake

Table 1. A subset of ciliated neurons fails to dye fill in *osta-1* mutants

	Percentage neurons filling with DiI					
Strain	ASH	ASJ	AWB	ASK	ADL	ASI
20°C						
Wild type	100	100	100	100	100	100
osta-1(oy98)	100	100	25	0	100	0
osta-1(ttTi4182)	100	100	29	2	100	0
osta-1(tm5255)	100	100	66	2	100	0
25°C						
Wild type	100	100	100	100	100	100
osta-1(oy98)	100	100	47	0	100	0
osta-1(ttTi4182)	100	100	54	0	100	0
osta-1(ttTi4182); Ex[osta-1 genomic]	100	100	100	100	100	87
osta-1(ttTi4182); Ex[osta-1 genomic::gfp]	100	100	100	100	100	90
osta-1(ttTi4182); Ex[srbc-66p::osta-1::mCherry]	100	100	75	100	100	0
osta-1(tm5255)	100	100	51	2	100	0

Adult animals were examined.
n=45-130 animals each.
All strains contain stably integrated copies of a *str-1p::gfp* fusion gene (*kyIs104*).

defect in *osta-1* mutants (Fig. 1D), whereas 80-100% of ADL, ASH and ASJ neurons filled with dye at all developmental stages examined (Fig. 1E; data not shown). Dye uptake in AWB and ASI was weaker and variable in young wild-type L1 larvae and thus could not be reliably quantified (data not shown). These results suggest that *osta-1* might be required to maintain the morphological integrity of ASK amphid sensory neurons.

osta-1 encodes a *C. elegans* homolog of the conserved eukaryotic organic solute transporter alpha protein

The dye-filling defects of *osta-1* mutants were rescued via germline-based transformation of sequences containing upstream regulatory and coding regions of the C01B12.4 gene (renamed *osta-1* here;

Fig. 1F; Table 1; data not shown). Topology analysis computed by TMHMM (http://www.cbs.dtu.dk/services/TMHMM/) (Krogh et al., 2001) suggests that OSTA-1 contains five transmembrane helices (Fig. 2A,B). The *C. elegans* genome is predicted to encode three additional members of this family, two of which (C18A3.4 and W01D2.5, herein named *osta-2* and *osta-3*, respectively) are closely related to OSTA-1 (supplementary material Fig. S1A).

The organic solute transporter protein family appears to be conserved across multiple eukaryotic species (Wang et al., 2001) (supplementary material Fig. S1A; see http://uswest.ensembl.org/Homo_sapiens/Gene/Compara_Tree?g=ENSG00000163959;r=3:195938358-195970049 for a detailed phylogenetic tree). Vertebrate organic solute transporter alpha (OSTα) proteins heterodimerize with OSTβ subunits to transport bile acids and steroids across the
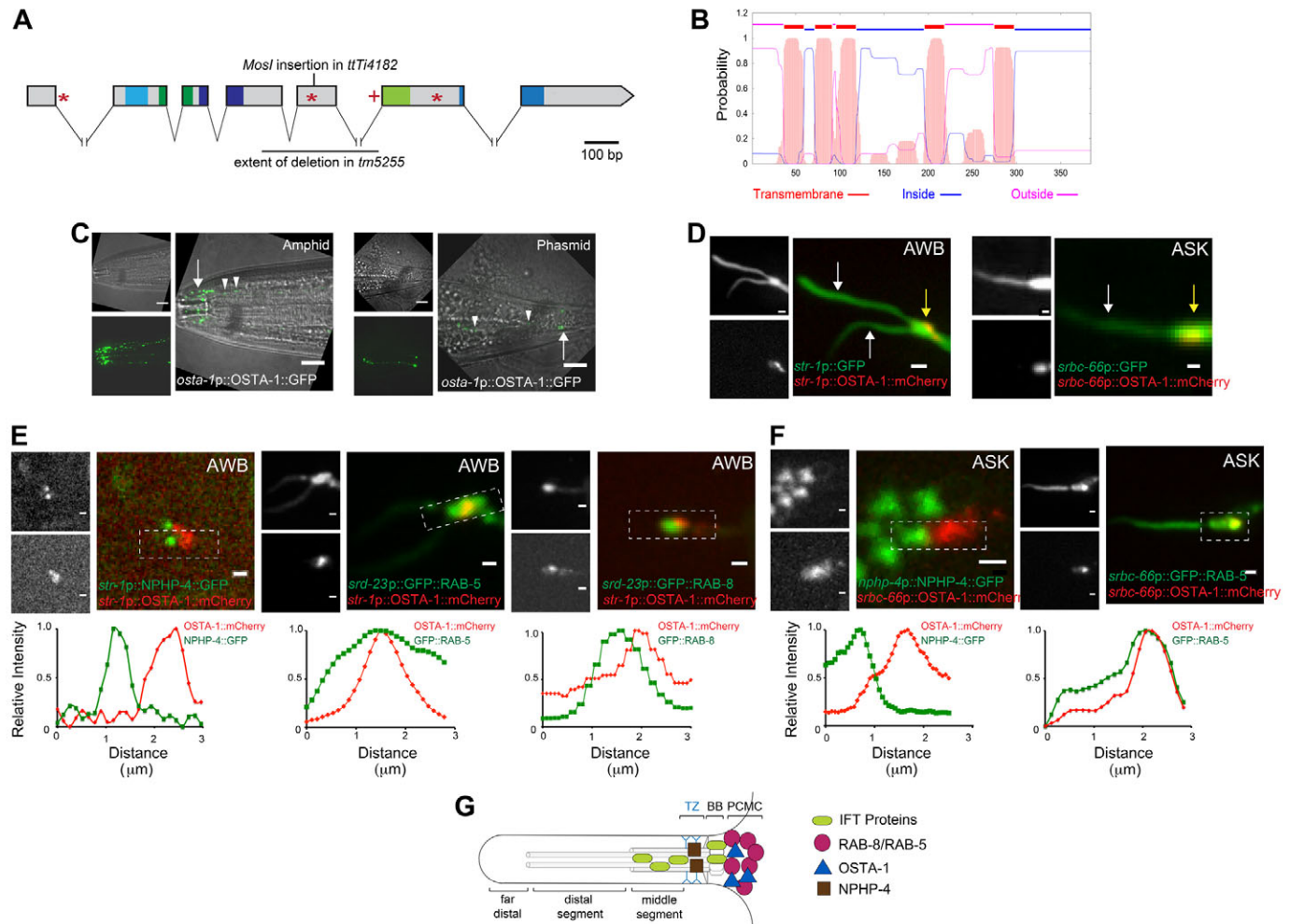

Fig. 2. *osta-1* encodes a transmembrane protein and is enriched in the periciliary compartments of ciliated neurons. (**A**) Predicted exon/intron structure of *C. elegans osta-1*. Filled boxes indicate sequences encoding predicted transmembrane domains. The extent of the deletion in *tm5255* and the site of *Mos1* transposon insertion in *ttTi4182* are indicated. Plus sign and asterisks indicate sites of nonsense codons in *in silico* translations of sequenced transcripts in *tm5255* and *ttTi4182* alleles, respectively (also see supplementary material Fig. S2). (**B**) Predicted transmembrane topology of OSTA-1 computed by TMHMM analysis. Plot shows posterior probabilities for the inside/outside/transmembrane domains. (**C**) GFP-tagged OSTA-1 protein expressed under its endogenous promoter is localized to sensory cilia base regions in the head amphid (left) and tail phasmid (right) organs (arrows). Note the punctate localization along dendrites in the head and tail (arrowheads). (**D**) Localization of OSTA-1::mCherry fusion protein at the ciliary base region of the AWB (left) and ASK (right) neurons. White and yellow arrows indicate cilia and dendrite, respectively. (**E,F**) Localization of OSTA-1::mCherry with the indicated fusion proteins in AWB (E) and ASK (F). Fluorescence intensities of fusion proteins are shown below each representative panel. The regions corresponding to the fluorescence intensity measurements are boxed (start is at left). Relative intensity was determined by subtracting the background pixel intensity and graphing as a fraction of the maximum pixel intensity. (**G**) Protein localization in a cilium (channel cilium or single AWB ciliary branch) and at the ciliary base (see Reiter et al., 2012). IFT, intraflagellar transport; TZ, transition zone; BB, basal body; PCMC, periciliary membrane trafficking compartment. Scale bars: 10 μm in C; 2 μm in D; 1 μm in E,F.

basolateral membrane (Ballatori et al., 2009; Dawson et al., 2010). However, invertebrate genomes do not appear to encode OSTβ, although this protein is poorly conserved even among vertebrates (Dawson et al., 2010). Other members of this larger protein family have previously been shown to be associated with membranes of intracellular vesicles and organelles such as endosomes and regulated secretory granules in *Arabidopsis* and mouse secretory tissues (Best and Adams, 2009; Best et al., 2008; Malinovsky et al., 2010), and the TMEM184a (SDMG1) protein has been suggested to play a role in post-Golgi membrane trafficking in Sertoli cells of mouse embryonic testes (Best et al., 2008). Similar to other family members, OSTA-1 may contain a potential di-leucine targeting motif implicated in the targeting of transmembrane proteins to endosomes and lysosomes (supplementary material Fig. S1B) (Bonifacino and Traub, 2003; Marks et al., 1996).

The molecular lesion in *oy98* is a large and complex deletion/rearrangement that we were unable to fully analyze by sequencing or amplification experiments. Sequences in the fourth and fifth exons of *osta-1* are deleted in *tm5255* (Fig. 2A). Sequence analyses of *osta-1* cDNAs in *tm5255* mutants indicated that the majority of predicted proteins are truncated before the fourth transmembrane domain (Fig. 2A; supplementary material Fig. S2). The *ttTi4182* mutation was isolated in a transposon-based mutagenesis screen (Bessereau et al., 2001; Granger et al., 2004) and sequencing showed insertion of the *Mos1* transposon into exon 5. The *ttTi4182* insertional mutation results in the generation of mutant cDNAs predicted to encode proteins that are truncated at variable locations or with deleted residues (Fig. 2A; supplementary material Fig. S2). Given the unknown nature and complexity of the *oy98* mutation, we chose to perform experiments with the *ttTi4182* and *tm5255* alleles.

OSTA-1 is expressed in amphid and phasmid ciliated neurons and is enriched in the periciliary membrane compartment

To examine the expression pattern of *osta-1*, we used a *gfp* transcriptional construct driven by 2.1 kb of *osta-1* upstream regulatory sequences. *gfp* expression was observed exclusively in all ciliated sensory neurons in the head amphid and tail phasmid organs, with occasional expression in other neurons (supplementary material Fig. S1C). Expression was observed at late embryonic stages and was maintained throughout postembryonic development. Consistent with its ciliated neuron-restricted expression pattern, *osta-1* is predicted to be regulated by the DAF-19 RFX transcription factor, a conserved regulator of ciliogenic genes (Chen et al., 2006; Phirke et al., 2011). *osta-2* and *osta-3* were also expressed neuronally, with expression in a subset of ciliated neurons, although expression was not restricted to these neuron types (supplementary material Fig. S1D). Previous reports have shown that the F40E10.6 homolog is also neuronally expressed and may be enriched at axons (Dolphin and Hope, 2006) (supplementary material Fig. S1D). No defects in dye filling were observed in *osta-2(tm5517)* and *osta-3(tm5460)* mutants (data not shown).

We next defined the subcellular localization of OSTA-1 in ciliated sensory neurons. A functional reporter-tagged OSTA-1 fusion protein (Table 1) expressed in the context of endogenous *osta-1* upstream and downstream regulatory sequences localized to the ciliary base region of expressing neurons (Fig. 2C). Localization to punctate structures was also observed along dendrites and axons and in cell bodies (Fig. 2C; not shown). OSTA-1::GFP was similarly present at the ciliary base region and as dendritic puncta when

expressed under the ASK-specific *srbc-66* or the AWB-specific *str-1* promoters (Fig. 2D; supplementary material Fig. S1E).

To examine OSTA-1 localization relative to subciliary domains, such as the transition zone, basal body compartment or the periciliary membrane trafficking compartment (PCMC) that is proximal to the basal body region (Kaplan et al., 2012; Reiter et al., 2012), we performed colocalization experiments. mCherry-tagged OSTA-1 was co-expressed with a GFP-tagged NPHP-4 transition zone protein (Williams et al., 2011), a GFP-tagged RAB-5 endocytic protein that is enriched in the PCMC (Kaplan et al., 2012) or with a GFP-tagged RAB-8 exocytic protein (Deretic et al., 1995; Kaplan et al., 2010). The OSTA-1 fusion protein was localized to a region that was proximal to, and did not overlap with, the transition zone housing NPHP-4 fusion proteins in either AWB or ASK, but instead colocalized with the RAB-5 fusion protein in both neuron types (Fig. 2E,F). Partial colocalization of the OSTA-1 fusion protein was also observed with GFP-tagged RAB-8 at the base of AWB cilia (Fig. 2E). Although the precise subcellular localization of OSTA-1 awaits higher resolution analyses, these data are consistent with enrichment of OSTA-1 to a region that is proximal to the transition zone and that overlaps with the PCMC (Fig. 2G), suggesting that OSTA-1 might play a role in the regulation of intracellular trafficking to, and/or from, the ciliary compartment.

OSTA-1 acts cell-autonomously to regulate the morphologies of specific cilia types

Since membrane trafficking proteins localized to the PCMC regulate cilia morphology (e.g. Dwyer et al., 2001; Hu et al., 2007; Kaplan et al., 2012; Kaplan et al., 2010; Nachury et al., 2007; Westlake et al., 2011), we further characterized possible ciliary phenotypes in *osta-1* mutants. Expression of *gfp* driven by the examined cell-specific promoters was unaffected in *osta-1* mutants, indicating that overall cell fate was unaltered (Fig. 3). However, we found that the lengths of ASK, ASH and ASI channel cilia were weakly but significantly affected in *osta-1* mutants in a temperature-dependent manner, suggesting an underlying temperature-sensitive process in the regulation of cilia length (Fig. 3A). Both ASK and ASI cilia in *osta-1* mutants were slightly shorter than in wild-type animals when cultivated at 25°C, but slightly longer when cultivated at 20°C (Fig. 3A). ASH cilia were slightly but significantly longer in *osta-1* mutants than in wild type regardless of growth temperature (Fig. 3A). Transmission electron microscopy analysis revealed that the ultrastructure of amphid channel cilia in *osta-1* mutants was grossly similar to that in wild-type controls (supplementary material Fig. S3). The transition zone and PCMC areas were also unaffected in *osta-1* mutants based on ultrastructural analyses of these areas (Fig. 3A; supplementary material Fig. S3).

Whereas the ASK and ASI cilia exhibit relatively simple rod-like structures, the specialized cilia of the AWA, AWB and AWC sensory neurons are unique and structurally complex (Perkins et al., 1986; Ward et al., 1975). The overall morphology of the AWA and AWC cilia did not appear to be affected in *osta-1* mutants (supplementary material Fig. S4); however, the AWB cilia exhibited significant morphological defects. In wild-type animals, the AWB cilia contain two branches of unequal length (Fig. 3B). In *osta-1* mutants, the length difference between the ciliary branches in AWB was exaggerated, largely owing to the shortening of one branch (Fig. 3B). As in the case of the channel cilia, the AWB cilia branch length phenotypes were temperature dependent, such that growth at the lower temperature of 20°C improved the length defect of the shorter AWB ciliary branch (Fig. 3B).
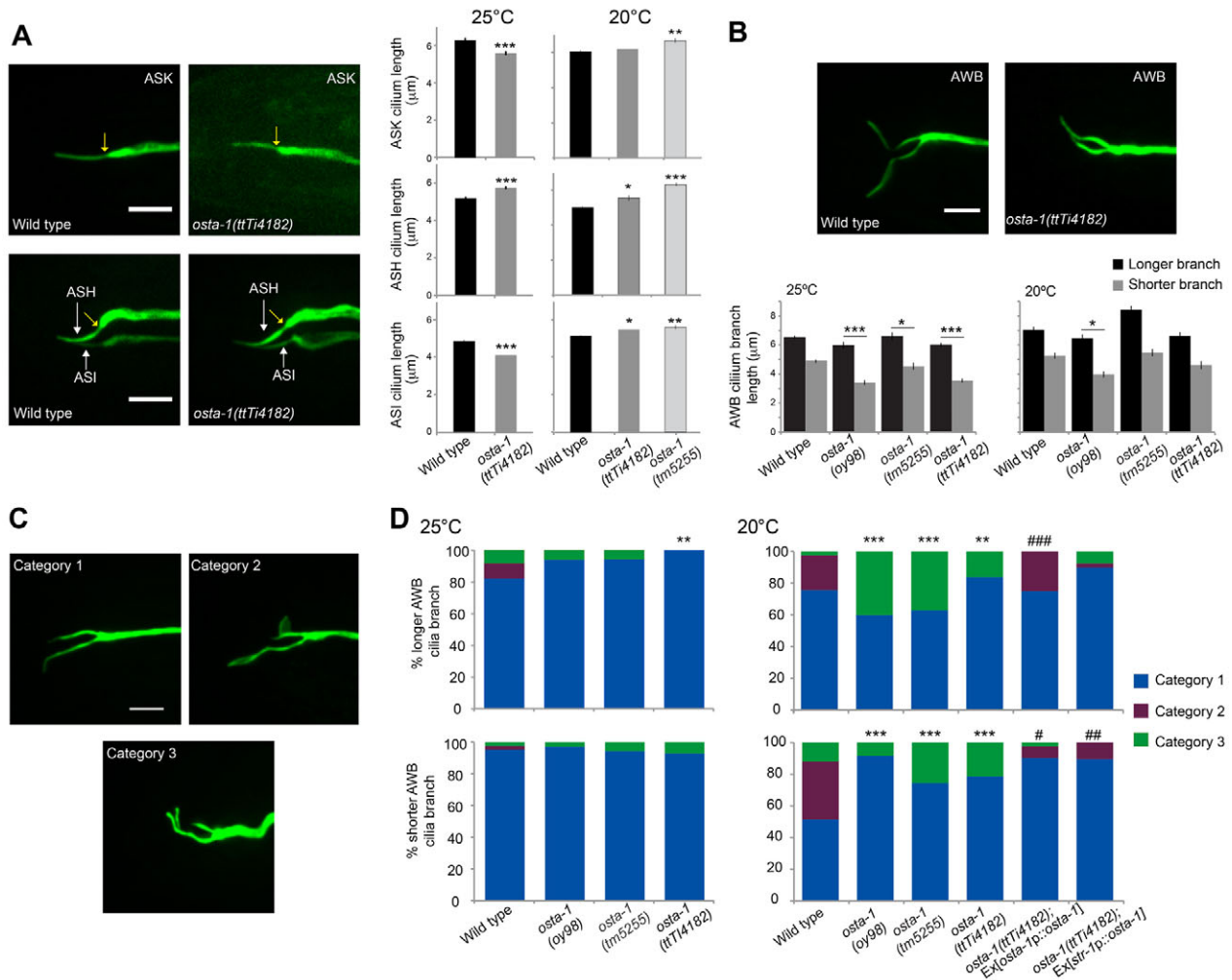
Fig. 3. *osta-1* mutants exhibit cell-specific cilia morphological defects. (**A**) ASK, ASH and ASI channel cilia in wild type and *osta-1* mutants visualized using *srbc-66*p::*gfp* (ASK) or *sra-6*p::*gfp* (ASH and ASI) transgenes. Yellow arrows indicate points at which length measurements (shown to the right) were initiated. *n*>29 cilia per data point. *$P<0.05$, **$P<0.01$, ***$P<0.001$, versus wild type (one-way ANOVA and Tukey's posthoc test). (**B**) *osta-1* mutants exhibit a shortened AWB ciliary branch. AWB cilia were visualized using the *str-1*p::*gfp* marker. *n*=30 cilia per measurement. *$P<0.05$, ***$P<0.001$, for ratios of shorter:longer branch lengths versus wild type (one-way ANOVA and Dunnett's posthoc test). (**C**) Representative images of AWB cilia in each category. Cilia were visualized using the *str-1*p::*gfp* marker. (**D**) Quantification of AWB cilia phenotypes in the indicated genetic backgrounds and growth temperatures. *n*≥30 cilia each. **$P<0.01$, ***$P<0.001$, versus wild type; #$P<0.05$, ##$P<0.01$, ###$P<0.001$, versus *osta-1(ttTl4182)* (crosstabs and chi-square test). Error bars indicate s.e.m. Scale bars: 5 μm.

In addition to the shortening of one branch, the AWB cilia in *osta-1* mutants exhibited other morphological defects. We previously showed that the area of the small membranous expansions ('fans') at the distal ends of AWB ciliary branches or along their lengths is variable even in wild-type animals, and that the fans are expanded in sensory signaling mutants and mutants with defects in trafficking (Kaplan et al., 2012; Mukhopadhyay et al., 2008). To quantitatively assess AWB cilia morphologies, we classified the AWB ciliary phenotypes into three categories that are similar, although not identical, to those described previously (Kaplan et al., 2012). Category 1 includes cilia with two primary branches and no fans; category 2 includes cilia with enlarged fans at either the distal end or along the primary branches; category 3 contains cilia with at least one secondary branch emanating from a ciliary primary branch (Fig. 3C). These quantifications were performed independently for the longer and shorter AWB cilia branches in wild type and *osta-1* mutants; the two branches exhibited qualitatively similar morphological phenotypes (Fig. 3D). We found that the AWB cilia

lacked all membranous fan-like areas in *osta-1* mutants regardless of growth temperature (Fig. 3D). In addition, ciliary branching was significantly increased when grown at 20°C (Fig. 3D).

Given the relatively broad expression pattern of *osta-1*, we next investigated whether *osta-1* acts cell-autonomously to regulate dye-filling and AWB ciliary morphological defects. Expression of a *osta-1* cDNA under the ASK-specific *srbc-66* promoter fully rescued the dye-filling defects of ASK in *osta-1* mutants without affecting the dye uptake defects in ASI (Fig. 1F; Table 1). Expression of genomic *osta-1* sequences or expression driven by the *str-1* promoter also partly restored the membranous fans in AWB cilia and reduced secondary branch numbers (Fig. 3D). Taken together, these results indicate that OSTA-1 acts cell-autonomously to regulate the morphologies of specific cilia types.

We next determined whether the observed ciliary morphological defects correlate with changes in IFT by quantifying the movement of functional GFP-tagged IFT-B particle component OSM-6 and of the OSM-3 and KAP-1 motor proteins in the cilia of ASH/ASI and

Table 2. IFT is weakly but significantly affected in AWB and ASH/ASI sensory cilia in *osta-1* mutants

| Fusion protein* | Strain background‡ | Mean velocity (µm/s ± s.d.) | | | |
		Middle segment	n/N§	Distal segment	n/N§
AWB					
OSM-6::GFP	Wild type	0.77±0.24	191/19	1.15±0.26	37/2
OSM-6::GFP	*osta-1*	0.73±0.20	314/22	0	0
KAP-1::GFP	Wild type	0.65±0.20	185/16	0.76±0.36	10/1
KAP-1::GFP	*osta-1*	0.65±0.25	170/15	0	0/0
OSM-3::GFP	Wild type	1.06±0.23	244/12	1.15±0.28	78/7
OSM-3::GFP	*osta-1*	0.90±0.29¶	258/20	1.05±0.17	7/2
ASH/ASI					
OSM-6::GFP	Wild type	0.80±0.22	234/9	1.12±0.34	212/9
OSM-6::GFP	*osta-1*	0.92±0.26¶	421/16	1.05±0.26#	496/16

Adult animals grown at 25°C were examined. Histograms of IFT velocities are shown in supplementary material Fig. S5.
*Fusion proteins were expressed under the *str-1* (AWB) or the *sra-6* (ASH/ASI) promoter.
‡The *osta-1(ttTI4182)* allele was used.
§*n*, number of particles; *N*, number of cilia.
¶Different from corresponding wild type at *P*<0.001.
#Different from corresponding wild type at *P*<0.05.

AWB neurons (Mukhopadhyay et al., 2007; Snow et al., 2004). Movement rates of OSM-3::GFP were significantly slower in the AWB cilia middle segments of *osta-1* mutants, with few or no transport events in the distal segments in either wild-type or *osta-1* mutant AWB cilia, as reported previously (Table 2; supplementary material Fig. S5) (Mukhopadhyay et al., 2007). However, OSM-6::GFP moved faster in the middle, and slower in the distal, segments of ASH/ASI cilia in *osta-1* mutants compared with wild-type animals (Table 2; supplementary material Fig. S5). Thus, loss of *osta-1* results in subtle, but significant, effects on IFT in the examined cilia in a cell type-specific manner.

The localization of a subset of ciliary transmembrane proteins is altered in a cell type-specific manner in *osta-1* mutants

Both exocytic and endocytic trafficking pathways are required for correct targeting and localization of ciliary proteins, including components of the core IFT machinery and ciliary transmembrane proteins (Ghossoub et al., 2011; Nachury et al., 2010; Pazour and Bloodgood, 2008; Qin, 2012). Since OSTA-1 may regulate intracellular trafficking, we next investigated whether loss of OSTA-1 function results in disruption of ciliary protein localization.

Consistent with previous observations, we noted ciliary localization of the SRBC-64 and SRG-36 G protein-coupled receptors (GPCRs) to the ASK and ASI cilia, respectively (Kim et al., 2009; McGrath et al., 2011), but also detected significant accumulation at the PCMC in wild-type animals (Fig. 4A,B; supplementary material Fig. S6A,B). In *osta-1* mutants, we observed increased accumulation of the SRBC-64 and SRG-36 fusion proteins at the PCMC in ASK and ASI, respectively (Fig. 4A-C; supplementary material Fig. S6A,B). Since the PCMC area in ASK or ASI cilia was not found to be increased when visualized with freely diffusible GFP in *osta-1* mutants (Fig. 3A), one interpretation of this phenotype is that the increased PCMC area is a secondary consequence of increased accumulation of overexpressed GPCRs in *osta-1* mutants. Unlike in the ASK neurons, localization of the STR-1 GPCR to the AWB cilia was unaffected in *osta-1* mutants (supplementary material Fig. S6C). By contrast, although a TAX-2::GFP cyclic nucleotide-gated channel fusion protein was enriched in the middle segments of ASK and AWB cilia in both wild type and *osta-1* mutants, we

observed some accumulation of this protein more proximally at the base of the cilia only in AWB in *osta-1* mutants (Fig. 4D,E; supplementary material Fig. S6D). Localization of the OSM-3 homodimeric kinesin motor, the KAP-1 heterotrimeric kinesin-II subunit and the OSM-6 IFT-B particle was unaffected in AWB and/or ASH/ASI cilia in *osta-1* mutants (supplementary material Fig. S6E-H). These results suggest that OSTA-1 might affect the localization of subsets of ciliary transmembrane, but not IFT, proteins in a cell-specific manner.

We next tested the hypothesis that the ciliary phenotypes of *osta-1* mutants arise from defects in the structure or function of the ciliary gate or diffusion barrier that maintains the cilia as a compartmentalized organelle. In *C. elegans*, this barrier is thought to comprise a large protein complex composed of MKS/MKSR/NPHP proteins that is localized to the transition zone (Bialas et al., 2009; Hu and Nelson, 2011; Huang et al., 2011; Jauregui and Barr, 2005; Reiter et al., 2012; Williams et al., 2011). The relative positions of NPHP-4 and MKSR-2 fusion proteins, as well as the transmembrane JBTS-14/TMEM237 and MKS-2/TMEM216 components at the transition zones, were grossly unaltered in *osta-1* mutants when expressed either cell-specifically in AWB and/or ASI neurons or in multiple ciliated neuron types (supplementary material Fig. S7A-E). Consistent with a lack of structural or morphological defects in the transition zone ultrastructure in *osta-1* mutants (supplementary material Fig. S3), the overall morphology of the transition zones as visualized by expression of transition zone fusion proteins was also unaltered in *osta-1* mutants (supplementary material Fig. S7A-E). These observations suggest that mutations in *osta-1* do not alter the overall organization and position of the transition zones or the localization of the transition zone proteins examined.

We next determined whether the diffusion kinetics of ciliary transmembrane proteins is altered in *osta-1* mutants by analyzing fluorescence recovery after photobleaching (FRAP). We used the ASI cilia-localized SRG-36::GFP GPCR fusion, which is mislocalized in *osta-1* mutants (Fig. 4A; supplementary material Fig. S6B). SRG-36::GFP was highly mobile within the ciliary compartment in both wild type and *osta-1* mutants, such that fluorescence recovered rapidly following photobleaching of a section of the ASI cilium (supplementary material Fig. S7F, Movies 1, 2) (Kaplan et al., 2012). Upon photobleaching the entire wild-type ASI cilium, SRG-36::GFP fluorescence levels recovered
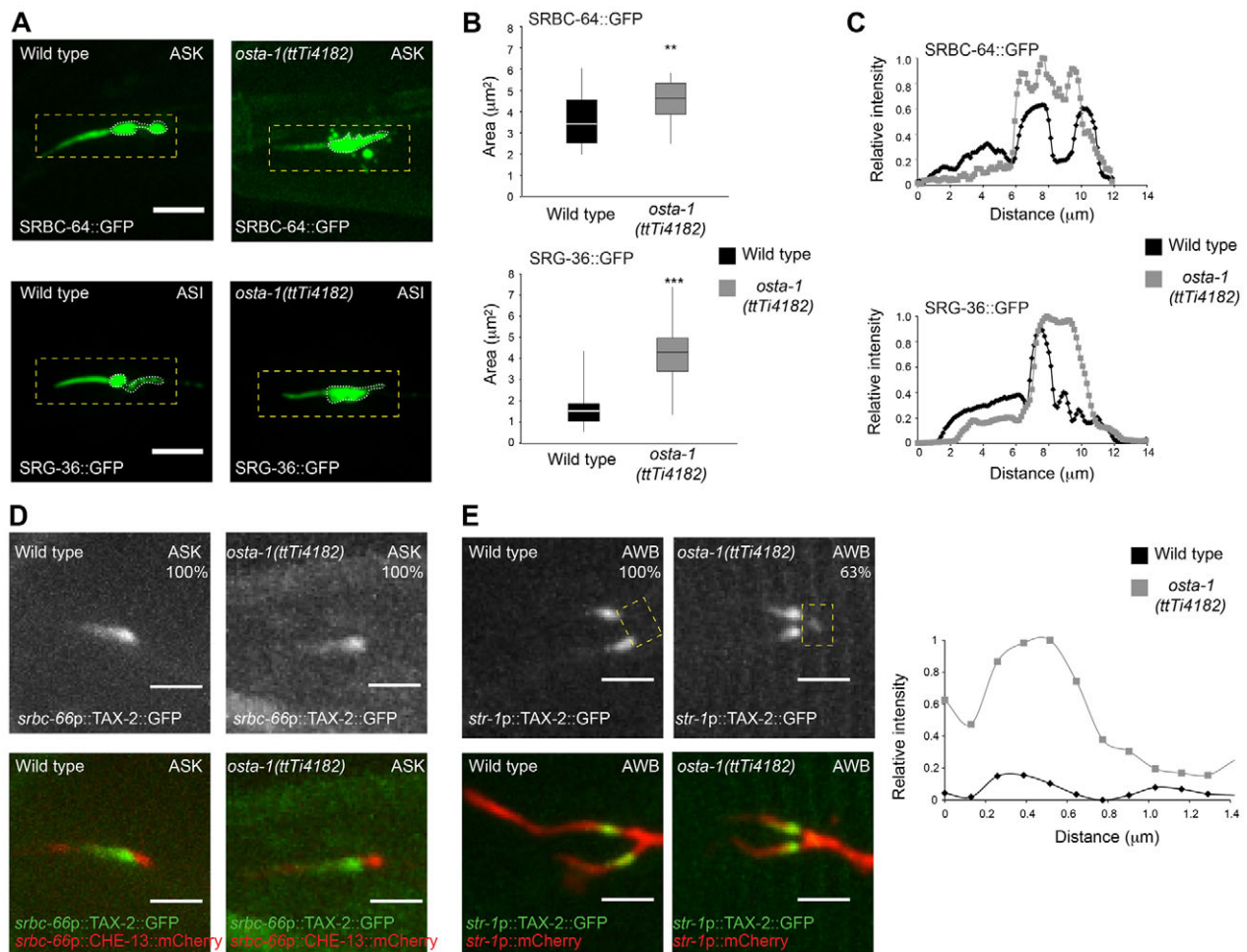
Fig. 4. Localization of a subset of ciliary transmembrane proteins is altered in *osta-1* mutants. (**A**) Localization of SRBC-64::GFP in ASK (top) and SRG-36::GFP in ASI (bottom) in the indicated genetic backgrounds. Expression in ASK and ASI was driven under the *srbc-64* and *str-3* promoters, respectively. Adult animals were grown at 25°C. (**B**) Quantification of total area of indicated fusion protein accumulation at the base of ASK and ASI cilia. Quantification in wild type and *osta-1* mutants grown at 20°C is shown in supplementary material Fig. S6A,B. The cilia base was manually outlined using ImageJ (indicated by dashed white lines in A). Horizontal lines indicate median; bottom and top boundaries of boxes indicate the 25th and 75th percentiles, respectively. Whiskers indicate the minimum and maximum values. Outliers (values greater or less than three standard deviations from the mean) are not shown. *n*=30 cilia each. **P<0.01, ***P<0.001, versus wild type. (**C**) Quantification of indicated fusion protein intensities across cilia and base of ASK and ASI (yellow boxes in A, start is at left). Data shown are from a single representative experiment. (**D,E**) Localization of TAX-2::GFP in ASK (D) and AWB (E) cilia. ASK and AWB cilia were visualized using *srbc-66*p::*che-13::mCherry* and *str-1*p::*mCherry*, respectively. Localization of TAX-2::GFP in AWB in *osta-1(tm5255)* mutants is shown in supplementary material Fig. S6D. Numbers at top right indicate the percentage of cilia exhibiting the phenotype; *n*≥20 each. Fluorescence intensities of fusion proteins measured in the boxed regions are shown in E (right). The data shown are from a single representative experiment. Scale bars: 5 μm in A; 2.5 μm in D,E.

partially and at a significantly slower rate (supplementary material Fig. S7G, Movie 3), suggesting the presence of a diffusion barrier at the ciliary base. Notably, neither the rate nor level of fluorescence recovery was altered in *osta-1* mutants (supplementary material Fig. S7G, Movie 4). Taken together, these observations indicate that the ciliary diffusion barrier in ASI is not grossly affected in *osta-1* mutants.

OSTA-1 interacts with intracellular trafficking pathways to regulate AWB cilia morphology

We previously suggested that ciliary membrane volume is regulated by a balance between membrane delivery via RAB-8/BBS-8–mediated exocytosis and membrane retrieval via AP-2-mediated endocytosis (Kaplan et al., 2012) (Fig. 5A). Moreover, genetic epistasis experiments suggested that sensory signaling might

regulate AWB ciliary morphology by regulation of exocytosis and endocytosis (Kaplan et al., 2012; Mukhopadhyay et al., 2008) (Fig. 5A). Since our data imply that OSTA-1 might regulate AWB cilia morphology by regulation of intracellular trafficking, we examined the genetic interaction of *osta-1* with components of the endocytic and exocytic pathways, as well as sensory signaling genes with respect to the AWB ciliary morphology phenotype.

Since loss of the *dpy-23* AP-2 adaptor μ2 subunit results in expanded AWB fans (Kaplan et al., 2012), whereas *osta-1* mutants lack all fans in the AWB cilia (Fig. 3D), we first determined whether *osta-1* is epistatic to *dpy-23* in regulating AWB cilia morphology. We found that the expanded fan in *dpy-23(e840)* animals was fully suppressed by *osta-1* mutations without any effects on branch length or complexity (Fig. 5B,C). Loss of sensory signaling as in *odr-1* receptor guanylyl cyclase mutants also results in large membranous
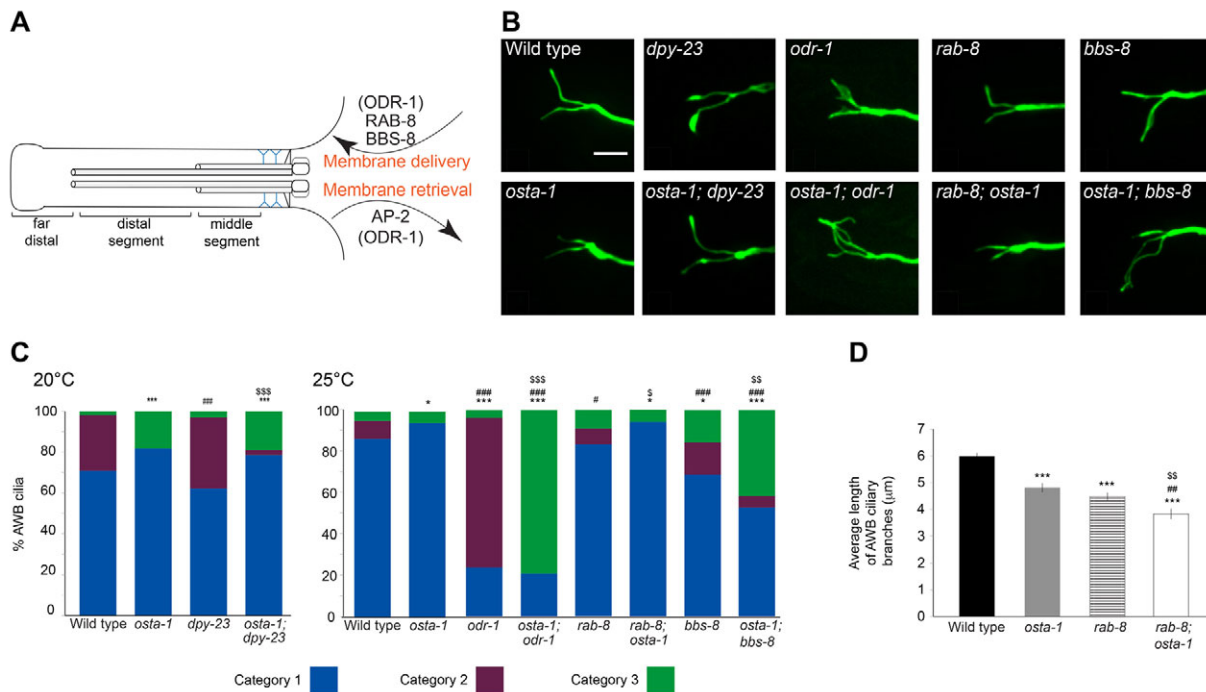
Fig. 5. OSTA-1 interacts with components of the exocytic and endocytic machinery to regulate AWB ciliary morphology. (A) Proteins implicated in regulating membrane homeostasis in AWB cilia. The role of sensory signaling mediated via ODR-1 is speculative; sensory signaling might modulate both ciliary membrane delivery and retrieval (see Kaplan et al., 2012). **(B)** Representative images of AWB cilia in the indicated genetic backgrounds. AWB cilia were visualized using the *str-1*p::*gfp* transgene. Scale bar: 5 μm. Alleles used were: *dpy-23(e840)*, *odr-1(n1936)*, *rab-8(tm2526)*, *bbs-8(nx77)* and *osta-1(ttTi4182)*. With the exception of strains containing *dpy-23(e840)*, which were examined at 20°C due to inviability at 25°C, all other strains were examined at 25°C. **(C)** Quantification of cilia phenotypes in the genetic backgrounds shown. Categories were defined as in Fig. 3C except that each AWB branch was considered independently (i.e. two measurements were obtained per AWB cilium). $n \geq 34$ cilia each. *$P<0.05$, ***$P<0.001$, versus wild type; #$P<0.05$, ###$P<0.001$, versus *osta-1*; $$$P<0.01$ and $$$$P<0.001$, versus corresponding second allele (one-way ANOVA and Bonferroni correction). **(D)** Average of both AWB cilia branch lengths in the indicated strains. $n \geq 35$ cilia per measurement. ***$P<0.001$, versus wild type; ##$P<0.01$, versus *osta-1*; $$$P<0.01$, versus *rab-8* (one-way ANOVA and Bonferroni correction). Error bars indicate s.e.m. Ratios of longer:shorter branch lengths were not significantly different from wild type. Adult animals were grown at 25°C.

fans in AWB (Mukhopadhyay et al., 2008). As in *osta-1;dpy-23* double mutants, the expanded fan phenotype in *odr-1* sensory signaling mutants was also fully suppressed by *osta-1* mutations (Fig. 5B,C). However, *osta-1;odr-1* double mutants exhibited phenotypes distinct from those of either single mutant or of *osta-1;dpy-23* double mutants (Fig. 5B,C), including extensive additional branching (Fig. 5B,C), suggesting a role for both sensory signaling and OSTA-1 in regulating branch complexity.

The expanded fan phenotype of endocytic and sensory signaling mutants is also suppressed by loss of *bbs-8* and *rab-8* functions (Kaplan et al., 2012; Mukhopadhyay et al., 2008). The AWB cilia phenotypes of double mutants between *osta-1* and *bbs-8/rab-8* were distinct from each other and from that of each single mutant. Whereas the AWB cilia in both double-mutant strains lacked extra membranous areas similar to *osta-1* single mutants, the predominant AWB cilia phenotype in *rab-8;osta-1* double mutants was proportional shortening of both AWB ciliary branches (Fig. 5B-D; data not shown), whereas the AWB cilia phenotype of *osta-1;bbs-8* double mutants was complex, with significantly increased branching compared with either single mutant (Fig. 5B,C). The results of the genetic epistasis experiments are most consistent with the hypothesis that OSTA-1 is crucial for membrane trafficking to or from the cilia, but that OSTA-1 also acts in distinct pathways with RAB-8 and BBS-8 to regulate axonemal structure (see Discussion).

A subset of OSTA-1 fusion proteins is mobile in the AWB dendrite and regulates RAB-5 trafficking

We and others have previously shown that the movement of proteins associated with exocytic or endocytic vesicles can be visualized in both retrograde and anterograde directions in *C. elegans* sensory neuron dendrites (Dwyer et al., 2001; Kaplan et al., 2012; Kaplan et al., 2010). We investigated whether OSTA-1 is mobile in the AWB dendrite, supporting possible vesicular association.

Time-lapse imaging of functional fluorescent reporter-tagged OSTA-1 protein showed both mobile and stationary OSTA-1::mCherry particles in the AWB dendrite, with more mobile particles moving in the retrograde than in the anterograde direction (Fig. 6A,C; supplementary material Table S3, Movie 5). OSTA-1 molecules exhibited both long-range translocation and short-range oscillatory movement along the dendrite with mean velocities within the range of motor-driven intracellular transport (mean anterograde velocity of 1.06±0.63 μm/s; mean retrograde velocity of 0.57±0.21 μm/s) (Fig. 6B; supplementary material Fig. S8A, Movie 5). The particles moved in a saltatory and bidirectional fashion, and included abrupt starts and stops and changes in direction (supplementary material Movie 5). The saltatory pattern of OSTA-1 movement resulted in highly variable individual track lengths, with 75% of the tracks being less than 3 μm in length (supplementary material Fig. S8B). All movement was abolished
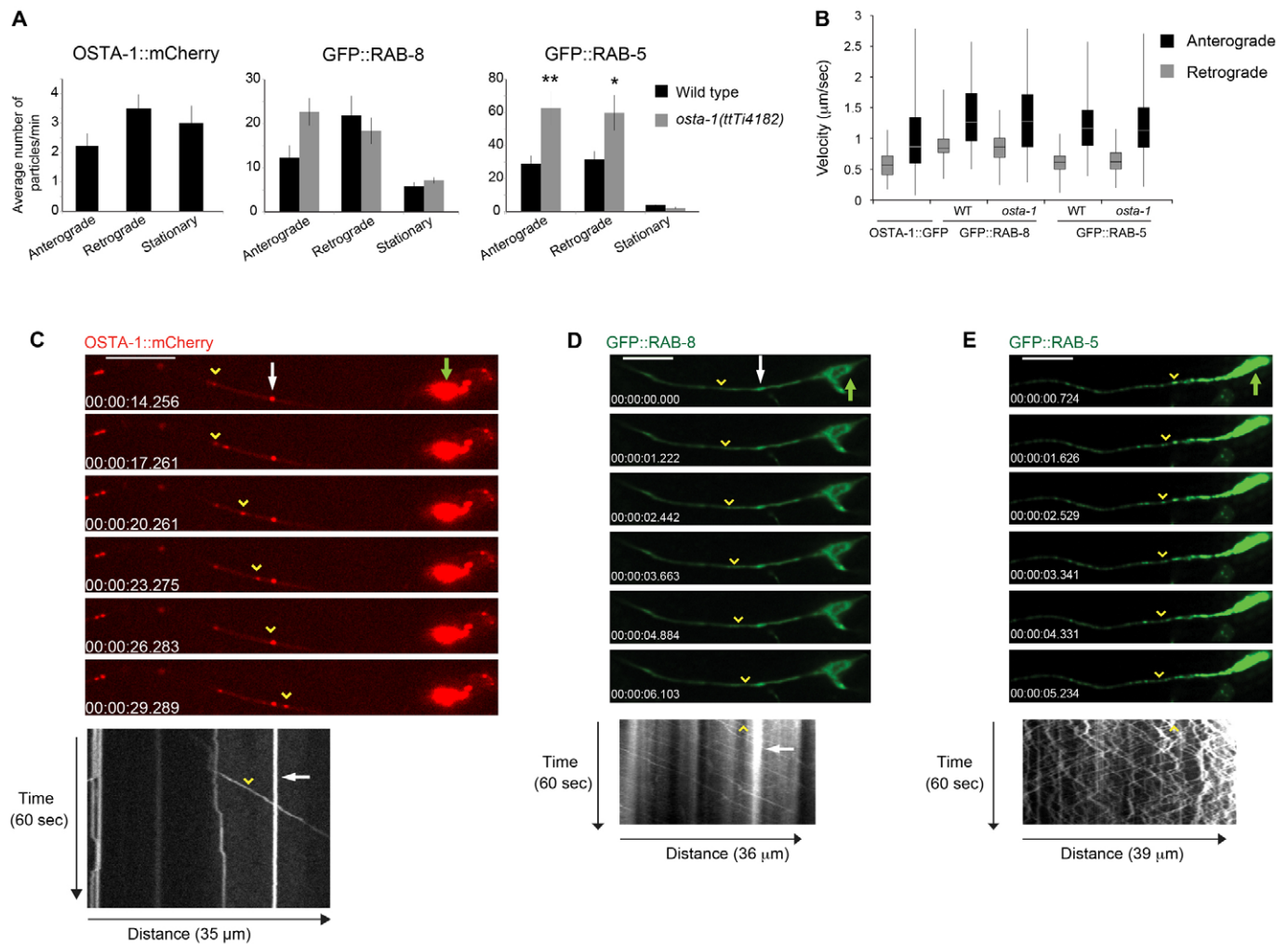
Fig. 6. OSTA-1 is mobile in AWB dendrites and regulates RAB-5 flux. (**A**) Flux of OSTA-1::GFP, GFP::RAB-8 and GFP::RAB-5 in the indicated backgrounds (see Materials and methods). For each data point, 7-15 kymographs were analyzed. *$P<0.05$, **$P<0.01$, versus wild type. Error bars indicate s.e. (**B**) Velocity distribution of fusion proteins in AWB dendrites in the indicated genetic backgrounds. Horizontal lines indicate median; lower and upper boundaries of box indicate 25th and 75th percentiles, respectively. Extent of whiskers indicates minimum and maximum values. Outliers (values greater or less than three standard deviations from the mean) are not included. n=81-468 particles; 7-15 animals each. Histograms of velocities are shown in supplementary material Fig. S8. (**C-E**) Still images from representative time-lapse series showing *str-1*p::OSTA-1::mCherry (C), *str-1*p::GFP::RAB-8 (D) and *str-1*p::GFP::RAB-5 (E) proteins in an AWB dendrite. Shown are six still images separated by 3 seconds (C) or 1 second (D,E). Anterior is left. Yellow arrowheads indicate movement of a single particle. White arrow indicates stationary particle (C,D); green arrows indicate AWB cell bodies. Kymographs of the series are shown beneath; images are aligned. Arrowheads and arrows in the kymographs indicate trajectories of stationary and mobile particles shown in still images above. A representative movie of OSTA-1::mCherry movement is shown in supplementary material Movie 5 and histograms of track lengths are shown in supplementary material Fig. S8. Scale bars: 10 μm.

upon exposure of animals to sodium azide, suggesting that transport was ATP dependent (data not shown).

Since OSTA-1 appears to partially colocalize with RAB-5 and RAB-8 at the PCMC, we examined whether OSTA-1 was associated with either protein in the AWB dendrite. As shown previously, a GFP::RAB-8 fusion protein moves robustly in the AWB dendrites (Fig. 6A,B,D; supplementary material Fig. S8) (Kaplan et al., 2012; Kaplan et al., 2010). We observed similar robust movement of a GFP::RAB-5 fusion protein in both the anterograde and retrograde direction (Fig. 6A,B,E; supplementary material Fig. S8). Unlike OSTA-1::GFP particles, the majority of GFP::RAB-8 and GFP::RAB-5 particles were mobile (Fig. 6A; supplementary material Table S3). Given the significantly higher number of mobile RAB-5 and RAB-8 particles as compared with mobile OSTA-1 particles observed in AWB dendrites

(supplementary material Table S3), we could not determine whether any observed association was due simply to chance. However, we noted that there was significant colocalization of OSTA-1 and RAB-5 in stationary particles (the observed frequency of colocalization in stationary particles was 0.014 particles/μm versus an expected frequency of 0.0036 particles/μm; $P<0.005$), suggesting an association between the two proteins.

We next investigated whether mutations in *osta-1* affect the trafficking dynamics of RAB-8 or RAB-5. Although the velocities of each protein were unaffected in *osta-1* mutants (Fig. 6B; supplementary material Fig. S8A), both the anterograde and retrograde flux of GFP::RAB-5 was markedly increased (Fig. 6A). Approximately twice as many RAB-5 particles were found to be mobile in both the anterograde and retrograde directions in *osta-1* mutants as in wild type (Fig. 6A). No significant effects were

observed on the flux of mobile GFP::RAB-8 (Fig. 6A). These observations suggest that OSTA-1 can be vesicle-associated and regulates the trafficking of RAB-5 vesicles in the AWB dendrite.

DISCUSSION

Our results suggest that OSTA-1 is a component of the membrane trafficking pathways that regulate sensory cilia morphology in *C. elegans*. This conclusion is based on several experimental observations. First, OSTA-1 is enriched at the PCMC, a specialized region at the ciliary base that is also enriched for membrane trafficking proteins (Hu et al., 2007; Kaplan et al., 2012). Second, OSTA-1 regulates the flux of anterograde and retrograde RAB-5 vesicles. Third, as shown previously for other trafficking mutants in *C. elegans* (Bae et al., 2006; Dwyer et al., 1998; Hu et al., 2007; Kaplan et al., 2012; Kaplan et al., 2010; Omori et al., 2008; Tan et al., 2007), the localization of a subset of ciliary transmembrane proteins is affected in *osta-1* mutants. Fourth, *osta-1* mutants lack all extraneous ciliary membranes in AWB, and mutations in *osta-1* are epistatic to all examined mutations in exocytic and endocytic genes with respect to the AWB ciliary membrane phenotype. Together with the observation that the ciliary gate is unaffected in *osta-1* mutants, these results are most consistent with the hypothesis that OSTA-1 regulates ciliary membrane and protein transport in part via regulation of trafficking of RAB-5-associated vesicles to and from the ciliary base.

Double-mutant combinations of *osta-1* with individual trafficking genes appear to affect different aspects of AWB ciliary morphology, such as membrane volume and branch length and complexity. For instance, *rab-8;osta-1* mutants exhibit truncated AWB ciliary branches, whereas *osta-1;odr-1* mutants exhibit increased branching. Increased trafficking of RAB-5-associated endocytic vesicles in *osta-1* mutants coupled with the disrupted delivery of ciliary components in *rab-8* mutants might result in AWB ciliary branch truncation in *rab-8;osta-1* double mutants. OSTA-1 might also link membrane trafficking to correct axonemal structure, as *osta-1* mutants alone exhibit increased branching at low temperatures. We have previously suggested that in sensory signaling mutants such as *odr-1*, compensatory overgrowth in AWB ciliary membrane volume maintains signaling homeostasis (Mukhopadhyay et al., 2008). We speculate that increased RAB-5 trafficking in *osta-1* mutants might preclude expansion of AWB membrane volume in sensory mutants, and that increased branching reflects an alternate homeostatic compensatory mechanism to increase overall AWB ciliary volume.

A role for OSTA-1-related proteins in regulating post-Golgi membrane trafficking might be conserved. In particular, OSTA-1-related proteins appear to be present in most, if not all, eukaryotic lineages, suggesting a possible fundamental role in regulating membrane transport. In mammals, expression of the distantly related TMEM184a protein appears to be restricted to secretory exocrine tissues, where the protein is associated with secretory granules and endosomes (Best and Adams, 2009; Best et al., 2008). Knocking down TMEM184a results in the mislocalization of a secretory SNARE protein in mouse Sertoli cell lines and in disruption of membrane trafficking and secretion (Best et al., 2008). We suggest that the stationary particles containing both RAB-5 and OSTA-1 might be localized membrane traffic 'control centers' similar to Golgi outposts (Hanus and Ehlers, 2008; Jan and Jan, 2010), and that interaction between RAB-5 and OSTA-1 in these centers modulates RAB-5 vesicle flux and contributes in part to the regulation of AWB cilia membrane content.

The association of OSTA-1 with a small subset of trafficked vesicles, as well as the effects of *osta-1* mutations on the localization of a restricted set of transmembrane proteins, suggest that OSTA-1 is also associated with vesicles transporting specific cargoes. One possibility is that OSTA-1 transports molecules to regulate the intralumenal milieu of vesicles, which in turn could influence aspects of vesicle function such as protein sorting, vesicle trafficking or fusion (Mellman et al., 1986; Scott and Gruenberg, 2011). Since bile acids are not found in invertebrates, it has been suggested that OSTα proteins might participate instead in the transport of steroids or eicasonoids in lower organisms (Dawson et al., 2010). Although OSTα and OSTβ are thought to act as obligate heterodimers for transport in vertebrates, the absence of OSTβ homologs in invertebrates suggests that OSTα might function on its own or with a different partner(s) in these organisms (Dawson et al., 2010). We did not detect gross defects in the sensory functions of affected neurons in *osta-1* mutants (see Materials and methods). Nevertheless, the relatively subtle ciliary defects of *osta-1* mutants might affect specific sensory behaviors under defined environmental conditions and genetic backgrounds (Huang et al., 2011; Jauregui and Barr, 2005; Williams et al., 2011; Williams et al., 2008) and have significant consequences for animal survival and fitness. A complete description of the role of OSTA-1 will require identification of the protein components of the associated vesicles and visualization of vesicle dynamics at the PCMC.

Finally, it is interesting to speculate on the cell-specific nature of *osta-1* mutant phenotypes. Only a subset of ciliated neurons fails to dye fill in *osta-1* mutants, the localization of different ciliary transmembrane proteins is affected in different neuron types, and the ciliary morphological defects and effects on IFT are neuron type specific. OSTA-1 might act partly redundantly with other related members of this family or other cell-specific factors to regulate ciliary morphology differentially in different cell types. This cell type specificity might also reflect distinct mechanisms by which axonemal morphology and membrane growth are coordinated in different neuron types, as well as the distinct ultrastructures and membrane compositions of functionally and morphologically distinct cilia (Pigino et al., 2012; Silverman and Leroux, 2009; Takeda and Narita, 2012). Thus, multiple molecular mechanisms might be employed in a combinatorial manner, both in an individual neuron as well as across different neuron types, to regulate the dynamic remodeling of cilia morphology. Given recent findings on the conservation of mechanisms by which cilia and polarized signaling centers, such as the immune synapse in non-ciliated cells, are formed (Baldari and Rosenbaum, 2010; Griffiths et al., 2010; Sedmak and Wolfrum, 2010), it is possible that different molecular components of trafficking pathways have been recruited to regulate cilia structures in specific cell types. Alternatively, the regulation of cilia structure might represent a diverged function for these proteins in invertebrates. Molecular diversity in remodeling pathways may allow regulation by diverse inputs, thereby ensuring that cilia architecture and function are sculpted appropriately for optimal cellular and organismal functions.

Competing interests statement
The authors declare no competing financial interests.

Supplementary material
Supplementary material available online at
http://dev.biologists.org/lookup/suppl/doi:10.1242/dev.086249/-/DC1

References
Avasthi, P. and Marshall, W. F. (2012). Stages of ciliogenesis and regulation of ciliary length. *Differentiation* **83**, S30-S42.
Bae, Y. K., Qin, H., Knobel, K. M., Hu, J., Rosenbaum, J. L. and Barr, M. M. (2006). General and cell-type specific mechanisms target TRPP2/PKD-2 to cilia. *Development* **133**, 3859-3870.
Baldari, C. T. and Rosenbaum, J. (2010). Intraflagellar transport: it's not just for cilia anymore. *Curr. Opin. Cell Biol.* **22**, 75-80.
Ballatori, N., Li, N., Fang, F., Boyer, J. L., Christian, W. V. and Hammond, C. L. (2009). OST alpha-OST beta: a key membrane transporter of bile acids and conjugated steroids. *Front. Biosci.* **14**, 2829-2844.
Bancaud, A., Huet, S., Rabut, G. and Ellenberg, J. (2010). Fluorescence perturbation techniques to study mobility and molecular dynamics of proteins in live cells: FRAP, photoactivation, photoconversion, and FLIP. *Cold Spring Harb. Protoc.* **2010**, doi:10.1101/pdb.top90.
Bargmann, C. I. and Horvitz, H. R. (1991). Control of larval development by chemosensory neurons in Caenorhabditis elegans. *Science* **251**, 1243-1246.
Bargmann, C. I., Thomas, J. H. and Horvitz, H. R. (1990). Chemosensory cell function in the behavior and development of Caenorhabditis elegans. *Cold Spring Harb. Symp. Quant. Biol.* **55**, 529-538.
Besschetnova, T. Y., Kolpakova-Hart, E., Guan, Y., Zhou, J., Olsen, B. R. and Shah, J. V. (2010). Identification of signaling pathways regulating primary cilium length and flow-mediated adaptation. *Curr. Biol.* **20**, 182-187.
Bessereau, J. L., Wright, A., Williams, D. C., Schuske, K., Davis, M. W. and Jorgensen, E. M. (2001). Mobilization of a Drosophila transposon in the Caenorhabditis elegans germ line. *Nature* **413**, 70-74.
Best, D. and Adams, I. R. (2009). Sdmg1 is a component of secretory granules in mouse secretory exocrine tissues. *Dev. Dyn.* **238**, 223-231.
Best, D., Sahlender, D. A., Walther, N., Peden, A. A. and Adams, I. R. (2008). Sdmg1 is a conserved transmembrane protein associated with germ cell sex determination and germline-soma interactions in mice. *Development* **135**, 1415-1425.
Bialas, N. J., Inglis, P. N., Li, C., Robinson, J. F., Parker, J. D., Healey, M. P., Davis, E. E., Inglis, C. D., Toivonen, T., Cottell, D. C. et al. (2009). Functional interactions between the ciliopathy-associated Meckel syndrome 1 (MKS1) protein and two novel MKS1-related (MKSR) proteins. *J. Cell Sci.* **122**, 611-624.
Bisgrove, B. W. and Yost, H. J. (2006). The roles of cilia in developmental disorders and disease. *Development* **133**, 4131-4143.
Bonifacino, J. S. and Traub, L. M. (2003). Signals for sorting of transmembrane proteins to endosomes and lysosomes. *Annu. Rev. Biochem.* **72**, 395-447.
Brenner, S. (1974). The genetics of Caenorhabditis elegans. *Genetics* **77**, 71-94.
Chen, N., Mah, A., Blacque, O. E., Chu, J., Phgora, K., Bakhoum, M. W., Newbury, C. R., Khattra, J., Chan, S., Go, A. et al. (2006). Identification of ciliary and ciliopathy genes in Caenorhabditis elegans through comparative genomics. *Genome Biol.* **7**, R126.
Czarnecki, P. G. and Shah, J. V. (2012). The ciliary transition zone: from morphology and molecules to medicine. *Trends Cell Biol.* **22**, 201-210.
Davis, M. W., Hammarlund, M., Harrach, T., Hullett, P., Olsen, S. and Jorgensen, E. M. (2005). Rapid single nucleotide polymorphism mapping in C. elegans. *BMC Genomics* **6**, 118.
Dawson, P. A., Hubbert, M. L. and Rao, A. (2010). Getting the mOST from OST: Role of organic solute transporter, OSTalpha-OSTbeta, in bile acid and steroid metabolism. *Biochim. Biophys. Acta* **1801**, 994-1004.
Deretic, D., Huber, L. A., Ransom, N., Mancini, M., Simons, K. and Papermaster, D. S. (1995). rab8 in retinal photoreceptors may participate in rhodopsin transport and in rod outer segment disk morphogenesis. *J. Cell Sci.* **108**, 215-224.
Dolphin, C. T. and Hope, I. A. (2006). Caenorhabditis elegans reporter fusion genes generated by seamless modification of large genomic DNA clones. *Nucleic Acids Res.* **34**, e72.
Dwyer, N. D., Troemel, E. R., Sengupta, P. and Bargmann, C. I. (1998). Odorant receptor localization to olfactory cilia is mediated by ODR-4, a novel membrane-associated protein. *Cell* **93**, 455-466.

Dwyer, N. D., Adler, C. E., Crump, J. G., L'Etoile, N. D. and Bargmann, C. I. (2001). Polarized dendritic transport and the AP-1 mu1 clathrin adaptor UNC-101 localize odorant receptors to olfactory cilia. *Neuron* **31**, 277-287.
Fisch, C. and Dupuis-Williams, P. (2011). Ultrastructure of cilia and flagella – back to the future! *Biol. Cell* **103**, 249-270.
Ghossoub, R., Molla-Herman, A., Bastin, P. and Benmerah, A. (2011). The ciliary pocket: a once-forgotten membrane domain at the base of cilia. *Biol. Cell* **103**, 131-144.
Goetz, S. C., Ocbina, P. J. and Anderson, K. V. (2009). The primary cilium as a Hedgehog signal transduction machine. *Methods Cell Biol.* **94**, 199-222.
Granger, L., Martin, E. and Ségalat, L. (2004). Mos as a tool for genome-wide insertional mutagenesis in Caenorhabditis elegans: results of a pilot study. *Nucleic Acids Res.* **32**, e117.
Griffiths, G. M., Tsun, A. and Stinchcombe, J. C. (2010). The immunological synapse: a focal point for endocytosis and exocytosis. *J. Cell Biol.* **189**, 399-406.
Hanus, C. and Ehlers, M. D. (2008). Secretory outposts for the local processing of membrane cargo in neuronal dendrites. *Traffic* **9**, 1437-1445.
Hedgecock, E. M., Culotti, J. G., Thomson, J. N. and Perkins, L. A. (1985). Axonal guidance mutants of Caenorhabditis elegans identified by filling sensory neurons with fluorescein dyes. *Dev. Biol.* **111**, 158-170.
Herman, R. K. and Hedgecock, E. M. (1990). Limitation of the size of the vulval primordium of Caenorhabditis elegans by lin-15 expression in surrounding hypodermis. *Nature* **348**, 169-171.
Higginbotham, H., Eom, T. Y., Mariani, L. E., Bachleda, A., Hirt, J., Gukassyan, V., Cusack, C. L., Lai, C., Caspary, T. and Anton, E. S. (2012). Arl13b in primary cilia regulates the migration and placement of interneurons in the developing cerebral cortex. *Dev. Cell* **23**, 925-938.
Hobert, O. (2002). PCR fusion-based approach to create reporter gene constructs for expression analysis in transgenic C. elegans. *Biotechniques* **32**, 728-730.
Hu, Q. and Nelson, W. J. (2011). Ciliary diffusion barrier: the gatekeeper for the primary cilium compartment. *Cytoskeleton (Hoboken)* **68**, 313-324.
Hu, J., Wittekind, S. G. and Barr, M. M. (2007). STAM and Hrs down-regulate ciliary TRP receptors. *Mol. Biol. Cell* **18**, 3277-3289.
Huang, L., Szymanska, K., Jensen, V. L., Janecke, A. R., Innes, A. M., Davis, E. E., Frosk, P., Li, C., Willer, J. R., Chodirker, B. N. et al. (2011). TMEM237 is mutated in individuals with a Joubert syndrome related disorder and expands the role of the TMEM family at the ciliary transition zone. *Am. J. Hum. Genet.* **89**, 713-730.
Hunnicutt, G. R., Kosfiszer, M. G. and Snell, W. J. (1990). Cell body and flagellar agglutinins in Chlamydomonas reinhardtii: the cell body plasma membrane is a reservoir for agglutinins whose migration to the flagella is regulated by a functional barrier. *J. Cell Biol.* **111**, 1605-1616.
Inglis, P. N., Ou, G., Leroux, M. R. and Scholey, J. M. (2007). The sensory cilia of Caenorhabditis elegans. *WormBook* **2007**, 1-22.
Jan, Y. N. and Jan, L. Y. (2010). Branching out: mechanisms of dendritic arborization. *Nat. Rev. Neurosci.* **11**, 316-328.
Jauregui, A. R. and Barr, M. M. (2005). Functional characterization of the C. elegans nephrocystins NPHP-1 and NPHP-4 and their role in cilia and male sensory behaviors. *Exp. Cell Res.* **305**, 333-342.
Jin, H., White, S. R., Shida, T., Schulz, S., Aguiar, M., Gygi, S. P., Bazan, J. F. and Nachury, M. V. (2010). The conserved Bardet-Biedl syndrome proteins assemble a coat that traffics membrane proteins to cilia. *Cell* **141**, 1208-1219.
Kaplan, O. I., Molla-Herman, A., Cevik, S., Ghossoub, R., Kida, K., Kimura, Y., Jenkins, P., Martens, J. R., Setou, M., Benmerah, A. et al. (2010). The AP-1 clathrin adaptor facilitates cilium formation and functions with RAB-8 in C. elegans ciliary membrane transport. *J. Cell Sci.* **123**, 3966-3977.
Kaplan, O. I., Doroquez, D. B., Cevik, S., Bowie, R. V., Clarke, L., Sanders, A. A., Kida, K., Rappoport, J. Z., Sengupta, P. and Blacque, O. E. (2012). Endocytosis genes facilitate protein and membrane transport in C. elegans sensory cilia. *Curr. Biol.* **22**, 451-460.
Ketting, R. F., Haverkamp, T. H., van Luenen, H. G. and Plasterk, R. H. (1999). Mut-7 of C. elegans, required for transposon silencing and RNA interference, is a homolog of Werner syndrome helicase and RNaseD. *Cell* **99**, 133-141.
Kim, K., Sato, K., Shibuya, M., Zeiger, D. M., Butcher, R. A., Ragains, J. R., Clardy, J., Touhara, K. and Sengupta, P. (2009). Two chemoreceptors mediate developmental effects of dauer pheromone in C. elegans. *Science* **326**, 994-998.
Kim, K., Kim, R. and Sengupta, P. (2010). The HMX/NKX homeodomain protein MLS-2 specifies the identity of the AWC sensory neuron type via regulation of the *ceh-36 Otx* gene in C. elegans. *Development* **137**, 963-974.
Krogh, A., Larsson, B., von Heijne, G. and Sonnhammer, E. L. (2001). Predicting transmembrane protein topology with a hidden Markov model: application to complete genomes. *J. Mol. Biol.* **305**, 567-580.
Lanjuin, A. and Sengupta, P. (2002). Regulation of chemosensory receptor expression and sensory signaling by the KIN-29 Ser/Thr kinase. *Neuron* **33**, 369-381.
Lechtreck, K. F., Johnson, E. C., Sakai, T., Cochran, D., Ballif, B. A., Rush, J., Pazour, G. J., Ikebe, M. and Witman, G. B. (2009). The Chlamydomonas

reinhardtii BBSome is an IFT cargo required for export of specific signaling proteins from flagella. *J. Cell Biol.* **187**, 1117-1132.

Liu, Q., Tan, G., Levenkova, N., Li, T., Pugh, E. N., Jr, Rux, J. J., Speicher, D. W. and Pierce, E. A. (2007). The proteome of the mouse photoreceptor sensory cilium complex. *Mol. Cell. Proteomics* **6**, 1299-1317.

Malinovsky, F. G., Brodersen, P., Fiil, B. K., McKinney, L. V., Thorgrimsen, S., Beck, M., Nielsen, H. B., Pietra, S., Zipfel, C., Robatzek, S. et al. (2010). Lazarus1, a DUF300 protein, contributes to programmed cell death associated with Arabidopsis acd11 and the hypersensitive response. *PLoS ONE* **5**, e12586.

Marks, M. S., Woodruff, L., Ohno, H. and Bonifacino, J. S. (1996). Protein targeting by tyrosine- and di-leucine-based signals: evidence for distinct saturable components. *J. Cell Biol.* **135**, 341-354.

Mayer, U., Ungerer, N., Klimmeck, D., Warnken, U., Schnölzer, M., Frings, S. and Möhrlen, F. (2008). Proteomic analysis of a membrane preparation from rat olfactory sensory cilia. *Chem. Senses* **33**, 145-162.

McGrath, P. T., Xu, Y., Ailion, M., Garrison, J. L., Butcher, R. A. and Bargmann, C. I. (2011). Parallel evolution of domesticated Caenorhabditis species targets pheromone receptor genes. *Nature* **477**, 321-325.

Mellman, I., Fuchs, R. and Helenius, A. (1986). Acidification of the endocytic and exocytic pathways. *Annu. Rev. Biochem.* **55**, 663-700.

Mesland, D. A., Hoffman, J. L., Caligor, E. and Goodenough, U. W. (1980). Flagellar tip activation stimulated by membrane adhesions in Chlamydomonas gametes. *J. Cell Biol.* **84**, 599-617.

Milenkovic, L., Scott, M. P. and Rohatgi, R. (2009). Lateral transport of Smoothened from the plasma membrane to the membrane of the cilium. *J. Cell Biol.* **187**, 365-374.

Moritz, O. L., Tam, B. M., Hurd, L. L., Peränen, J., Deretic, D. and Papermaster, D. S. (2001). Mutant rab8 Impairs docking and fusion of rhodopsin-bearing post-Golgi membranes and causes cell death of transgenic Xenopus rods. *Mol. Biol. Cell* **12**, 2341-2351.

Mukhopadhyay, S., Lu, Y., Qin, H., Lanjuin, A., Shaham, S. and Sengupta, P. (2007). Distinct IFT mechanisms contribute to the generation of ciliary structural diversity in C. elegans. *EMBO J.* **26**, 2966-2980.

Mukhopadhyay, S., Lu, Y., Shaham, S. and Sengupta, P. (2008). Sensory signaling-dependent remodeling of olfactory cilia architecture in C. elegans. *Dev. Cell* **14**, 762-774.

Nachury, M. V., Loktev, A. V., Zhang, Q., Westlake, C. J., Peränen, J., Merdes, A., Slusarski, D. C., Scheller, R. H., Bazan, J. F., Sheffield, V. C. et al. (2007). A core complex of BBS proteins cooperates with the GTPase Rab8 to promote ciliary membrane biogenesis. *Cell* **129**, 1201-1213.

Nachury, M. V., Seeley, E. S. and Jin, H. (2010). Trafficking to the ciliary membrane: how to get across the periciliary diffusion barrier? *Annu. Rev. Cell Dev. Biol.* **26**, 59-87.

Omori, Y., Zhao, C., Saras, A., Mukhopadhyay, S., Kim, W., Furukawa, T., Sengupta, P., Veraksa, A. and Malicki, J. (2008). Elipsa is an early determinant of ciliogenesis that links the IFT particle to membrane-associated small GTPase Rab8. *Nat. Cell Biol.* **10**, 437-444.

Orozco, J. T., Wedaman, K. P., Signor, D., Brown, H., Rose, L. and Scholey, J. M. (1999). Movement of motor and cargo along cilia. *Nature* **398**, 674.

Ou, G., Koga, M., Blacque, O. E., Murayama, T., Ohshima, Y., Schafer, J. C., Li, C., Yoder, B. K., Leroux, M. R. and Scholey, J. M. (2007). Sensory ciliogenesis in Caenorhabditis elegans: assignment of IFT components into distinct modules based on transport and phenotypic profiles. *Mol. Biol. Cell* **18**, 1554-1569.

Pan, J. and Snell, W. J. (2005). Chlamydomonas shortens its flagella by activating axonemal disassembly, stimulating IFT particle trafficking, and blocking anterograde cargo loading. *Dev. Cell* **9**, 431-438.

Papermaster, D. S., Schneider, B. G. and Besharse, J. C. (1985). Vesicular transport of newly synthesized opsin from the Golgi apparatus toward the rod outer segment. Ultrastructural immunocytochemical and autoradiographic evidence in Xenopus retinas. *Invest. Ophthalmol. Vis. Sci.* **26**, 1386-1404.

Pazour, G. J. and Bloodgood, R. A. (2008). Targeting proteins to the ciliary membrane. *Curr. Top. Dev. Biol.* **85**, 115-149.

Pedersen, L. B., Veland, I. R., Schrøder, J. M. and Christensen, S. T. (2008). Assembly of primary cilia. *Dev. Dyn.* **237**, 1993-2006.

Perkins, L. A., Hedgecock, E. M., Thomson, J. N. and Culotti, J. G. (1986). Mutant sensory cilia in the nematode Caenorhabditis elegans. *Dev. Biol.* **117**, 456-487.

Phirke, P., Efimenko, E., Mohan, S., Burghoorn, J., Crona, F., Bakhoum, M. W., Trieb, M., Schuske, K., Jorgensen, E. M., Piasecki, B. P. et al. (2011). Transcriptional profiling of C. elegans DAF-19 uncovers a ciliary base-associated protein and a CDK/CCRK/LF2p-related kinase required for intraflagellar transport. *Dev. Biol.* **357**, 235-247.

Pigino, G., Maheshwari, A., Bui, K. H., Shingyoji, C., Kamimura, S. and Ishikawa, T. (2012). Comparative structural analysis of eukaryotic flagella and cilia from Chlamydomonas, Tetrahymena, and sea urchins. *J. Struct. Biol.* **178**, 199-206.

Qin, H. (2012). Regulation of intraflagellar transport and ciliogenesis by small G proteins. *Int. Rev. Cell Mol. Biol.* **293**, 149-168.

Reiter, J. F., Blacque, O. E. and Leroux, M. R. (2012). The base of the cilium: roles for transition fibres and the transition zone in ciliary formation, maintenance and compartmentalization. *EMBO Rep.* **13**, 608-618.

Rosenbaum, J. L. and Witman, G. B. (2002). Intraflagellar transport. *Nat. Rev. Mol. Cell Biol.* **3**, 813-825.

Sarafi-Reinach, T. R., Melkman, T., Hobert, O. and Sengupta, P. (2001). The lin-11 LIM homeobox gene specifies olfactory and chemosensory neuron fates in C. elegans. *Development* **128**, 3269-3281.

Satir, P. and Christensen, S. T. (2007). Overview of structure and function of mammalian cilia. *Annu. Rev. Physiol.* **69**, 377-400.

Scott, C. C. and Gruenberg, J. (2011). Ion flux and the function of endosomes and lysosomes: pH is just the start: the flux of ions across endosomal membranes influences endosome function not only through regulation of the luminal pH. *BioEssays* **33**, 103-110.

Sedmak, T. and Wolfrum, U. (2010). Intraflagellar transport molecules in ciliary and nonciliary cells of the retina. *J. Cell Biol.* **189**, 171-186.

Silverman, M. A. and Leroux, M. R. (2009). Intraflagellar transport and the generation of dynamic, structurally and functionally diverse cilia. *Trends Cell Biol.* **19**, 306-316.

Singla, V. and Reiter, J. F. (2006). The primary cilium as the cell's antenna: signaling at a sensory organelle. *Science* **313**, 629-633.

Snow, J. J., Ou, G., Gunnarson, A. L., Walker, M. R., Zhou, H. M., Brust-Mascher, I. and Scholey, J. M. (2004). Two anterograde intraflagellar transport motors cooperate to build sensory cilia on C. elegans neurons. *Nat. Cell Biol.* **6**, 1109-1113.

Sorokin, S. (1962). Centrioles and the formation of rudimentary cilia by fibroblasts and smooth muscle cells. *J. Cell Biol.* **15**, 363-377.

Starich, T. A., Herman, R. K., Kari, C. K., Yeh, W.-H., Schackwitz, W. S., Schuyler, M. W., Collet, J., Thomas, J. H. and Riddle, D. L. (1995). Mutations affecting the chemosensory neurons of Caenorhabditis elegans. *Genetics* **139**, 171-188.

Svingen, T., Beverdam, A., Bernard, P., McClive, P., Harley, V. R., Sinclair, A. H. and Koopman, P. (2007). Sex-specific expression of a novel gene Tmem184a during mouse testis differentiation. *Reproduction* **133**, 983-989.

Takeda, S. and Narita, K. (2012). Structure and function of vertebrate cilia, towards a new taxonomy. *Differentiation* **83**, S4-S11.

Tan, P. L., Barr, T., Inglis, P. N., Mitsuma, N., Huang, S. M., Garcia-Gonzalez, M. A., Bradley, B. A., Coforio, S., Albrecht, P. J., Watnick, T. et al. (2007). Loss of Bardet Biedl syndrome proteins causes defects in peripheral sensory innervation and function. *Proc. Natl. Acad. Sci. USA* **104**, 17524-17529.

Troemel, E. R., Kimmel, B. E. and Bargmann, C. I. (1997). Reprogramming chemotaxis responses: sensory neurons define olfactory preferences in C. elegans. *Cell* **91**, 161-169.

van der Linden, A. M., Nolan, K. M. and Sengupta, P. (2007). KIN-29 SIK regulates chemoreceptor gene expression via an MEF2 transcription factor and a class II HDAC. *EMBO J.* **26**, 358-370.

Wang, W., Seward, D. J., Li, L., Boyer, J. L. and Ballatori, N. (2001). Expression cloning of two genes that together mediate organic solute and steroid transport in the liver of a marine vertebrate. *Proc. Natl. Acad. Sci. USA* **98**, 9431-9436.

Ward, S., Thomson, N., White, J. G. and Brenner, S. (1975). Electron microscopical reconstruction of the anterior sensory anatomy of the nematode Caenorhabditis elegans.?2UU. *J. Comp. Neurol.* **160**, 313-337.

Westlake, C. J., Baye, L. M., Nachury, M. V., Wright, K. J., Ervin, K. E., Phu, L., Chalouni, C., Beck, J. S., Kirkpatrick, D. S., Slusarski, D. C. et al. (2011). Primary cilia membrane assembly is initiated by Rab11 and transport protein particle II (TRAPPII) complex-dependent trafficking of Rabin8 to the centrosome. *Proc. Natl. Acad. Sci. USA* **108**, 2759-2764.

Williams, C. L., Winkelbauer, M. E., Schafer, J. C., Michaud, E. J. and Yoder, B. K. (2008). Functional redundancy of the B9 proteins and nephrocystins in Caenorhabditis elegans ciliogenesis. *Mol. Biol. Cell* **19**, 2154-2168.

Williams, C. L., Li, C., Kida, K., Inglis, P. N., Mohan, S., Semenec, L., Bialas, N. J., Stupay, R. M., Chen, N., Blacque, O. E. et al. (2011). MKS and NPHP modules cooperate to establish basal body/transition zone membrane associations and ciliary gate function during ciliogenesis. *J. Cell Biol.* **192**, 1023-1041.